

## Multiscale modeling of reinforced/prestressed concrete thin-walled structures

Arghadeep Laskar<sup>1</sup>, Jianxia Zhong<sup>2</sup>, Y.L. Mo<sup>1\*</sup> and Thomas T.C. Hsu<sup>1</sup>

<sup>1</sup>*Department of Civil and Environmental Engineering, University of Houston, Houston, 77204-4003, USA*

<sup>2</sup>*MMI Engineering Inc., Houston, Texas, USA*

*(Received December 19, 2007, Accepted August 15, 2008)*

**Abstract.** Reinforced and prestressed concrete (RC and PC) thin walls are crucial to the safety and serviceability of structures subjected to shear. The shear strengths of elements in walls depend strongly on the softening of concrete struts in the principal compression direction due to the principal tension in the perpendicular direction. The past three decades have seen a rapid development of knowledge in shear of reinforced concrete structures. Various rational models have been proposed that are based on the smeared-crack concept and can satisfy Navier's three principles of mechanics of materials (i.e., stress equilibrium, strain compatibility and constitutive laws). The Cyclic Softened Membrane Model (CSMM) is one such rational model developed at the University of Houston, which is being efficiently used to predict the behavior of RC/PC structures critical in shear. CSMM for RC has already been implemented into finite element framework of OpenSees (Fenves 2005) to come up with a finite element program called Simulation of Reinforced Concrete Structures (SRCS) (Zhong 2005, Mo *et al.* 2008). CSMM for PC is being currently implemented into SRCS to make the program applicable to reinforced as well as prestressed concrete. The generalized program is called Simulation of Concrete Structures (SCS). In this paper, the CSMM for RC/PC in material scale is first introduced. Basically, the constitutive relationships of the materials, including uniaxial constitutive relationship of concrete, uniaxial constitutive relationships of reinforcements embedded in concrete and constitutive relationship of concrete in shear, are determined by testing RC/PC full-scale panels in a Universal Panel Tester available at the University of Houston. The formulation in element scale is then derived, including equilibrium and compatibility equations, relationship between biaxial strains and uniaxial strains, material stiffness matrix and RC plane stress element. Finally the formulated results with RC/PC plane stress elements are implemented in structure scale into a finite element program based on the framework of OpenSees to predict the structural behavior of RC/PC thin-walled structures subjected to earthquake-type loading. The accuracy of the multiscale modeling technique is validated by comparing the simulated responses of RC shear walls subjected to reversed cyclic loading and shake table excitations with test data. The response of a post tensioned precast column under reversed cyclic loads has also been simulated to check the accuracy of SCS which is currently under development. This multiscale modeling technique greatly improves the simulation capability of RC thin-walled structures available to researchers and engineers.

**Keywords:** multiscale modeling; reinforced concrete; thin-walled structure; constitutive law; nonlinear finite element.

---

\* Corresponding Author, Email: [yomo@uh.edu](mailto:yomo@uh.edu)

## 1. Introduction

The past three decades have seen a rapid development of knowledge in shear of reinforced concrete structures. Various rational models have been proposed that are based on the smeared-crack concept and can satisfy Navier's three principles of mechanics of materials (i.e., stress equilibrium, strain compatibility and constitutive laws). These rational or mechanics-based models on the "smeared-crack level" (in contrast to the "discrete-crack level" or "local level") include the compression field theory (CFT) (Vecchio and Collins 1981), the modified compression field theory (MCFT) (Vecchio and Collins 1986), the rotating-angle softened truss model, (RA-STM) (Hsu 1993, Belarbi and Hsu 1995, Pang and Hsu 1995), the fixed-angle softened truss model, (FA-STM) (Pang and Hsu 1996, Hsu and Zhang 1996), the softened membrane model, (SMM) (Zhu 2000, Hsu and Zhu 2002), and the cyclic softened membrane model, (CSMM) (Mansour 2001, Mansour and Hsu 2005a, 2005b, Hsu and Mansour 2005).

Vecchio and Collins (1981) proposed the earliest rational theory CFT, to predict the nonlinear behavior of cracked reinforced concrete membrane elements. However, the CFT was unable to take into account the tension stiffening of the concrete in the prediction of deformations because the tensile stress of concrete was assumed to be zero. In 1986 the MCFT was proposed to include a relationship for concrete in tension to better model the stiffness of experiments.

The RA-STM, a rational theory developed at the University of Houston (UH) in 1995, had two improvements over the CFT: (1) The tensile stress of concrete was taken into account so that the deformations could be correctly predicted, and (2) the smeared (or average) stress-strain curve of steel bars embedded in concrete was derived on the "smeared crack level" so that it could be correctly used in the equilibrium and compatibility equations which are based on continuous materials.

By 1996 the UH group reported the FA-STM that is capable of predicting the "concrete contribution" ( $V_c$ ) by assuming the cracks to be oriented at the fixed angle. Zhu *et al.* (2001) derived a rational shear modulus and produced a solution algorithm of FA-STM that is as simple as that of RA-STM.

Another significant advancement has come with the improvements on the softened truss models (rotating-angle and fixed-angle). As they were, these models could predict the ascending response curves of shear panels, but not the post-peak descending curves. By incorporating the Poisson effect of cracked reinforced concrete (characterized by two new Hsu/Zhu ratios), the Softened Membrane Model (SMM) was developed which can satisfactorily predict the entire monotonic response curves, including both the ascending and descending branches.

Fifteen reinforced concrete elements (panels) under reversed cyclic shear stresses, were tested by Mansour and Hsu (2005a, 2005b). Based on these test results, the Cyclic Softened Membrane Model (CSMM) was proposed to rationally predict the hysteretic loops of reinforced concrete. The CSMM can accurately predict the pinching effect, the shear ductility and the energy dissipation capacities of the membrane element (Hsu and Mansour 2005). For these reasons, The CSMM is the most appropriate model to be implemented in the OpenSees platform (Fenves 2005) for the prediction of the cyclic shear force-displacement behavior of walls where shear deformations are significant. In recent years the SMM has also been extended to prestressed concrete (PC) to develop the SMM-PC (Wang 2006). This can be used in conjunction with the CSMM to rationally predict the hysteresis loops for prestressed concrete structures.

In this paper, the SMM-PC in material scale is first introduced along with the cyclic behavior of

the materials as obtained from the CSMM. It basically includes the constitutive relationships of the materials, including uniaxial constitutive relationship of concrete, uniaxial constitutive relationships of mild steel bars and prestressing tendons embedded in concrete and constitutive relationship of concrete in shear that were determined by testing full-scale panels in a Universal Panel Tester available at UH. The formulation in element scale is then derived, including equilibrium and compatibility equations, relationship between biaxial strains and uniaxial strains, material stiffness matrix and RC plane stress element. Finally the formulated results with RC plane stress elements are implemented into a finite element program based on the framework of OpenSees (Fenves 2005) to predict the structural scale behavior of RC thin-walled structures subjected to earthquake-type loading. The accuracy of the multiscale modeling technique is validated by comparing the simulated responses of RC shear walls subjected to reversed cyclic loading and shake table excitation with test data.

## 2. Material scale

In this section the material constitutive laws of concrete, reinforcing bars, and prestressing tendons as developed at UH in the past twenty years using the Universal Panel Tester (Fig. 1), are described. The cyclic behavior of these materials as obtained from the CSMM has also been incorporated herein. It should be noted that the CSMM has been developed for RC and does not contain the cyclic behavior of prestressing tendons. Hence the cyclic behavior of reinforcing bars has been extended to the prestressing tendons. The coordinate systems followed in the development of the constitutive laws are shown in Fig. 2. Coordinate  $x$ - $y$  represents the local coordinate of the elements. The coordinate 1-2 defines the principal stress directions of the applied stresses, which have an angle  $\theta_1$  with respect to the  $x$ - axis. Steel bars can be oriented in different directions in the elements. Coordinate  $x_{si}$ - $y_{si}$  shows the direction of the ' $i$ th' group of rebars, where the ' $i$ th' group of rebars are located in the direction of axis  $x_{si}$  with an angle  $\theta_{si}$  to the  $x$ - axis.

### 2.1 Constitutive relationships of concrete in reinforced/prestressed element

The constitutive relationships for the tensile stress  $\sigma_1^c$  versus uniaxial tensile strain  $\bar{\epsilon}_1$  of concrete



Fig. 1 Universal panel tester

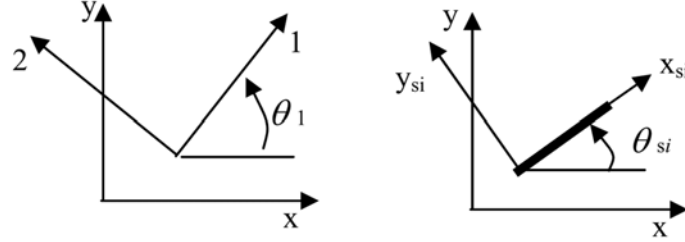


Fig. 2 Coordinate systems for reinforced concrete elements (A) applied principal stresses in local coordinate (B) reinforcement component in local coordinate

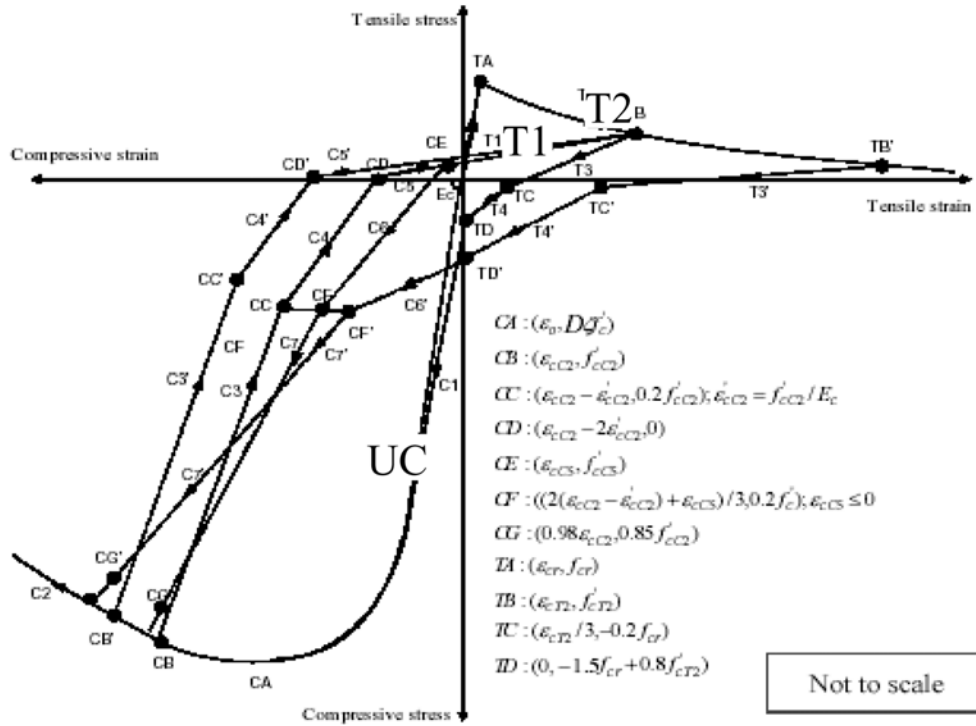


Fig. 3 Cyclic smeared stress-strain curves of prestressed concrete

under prestress (Fig. 3) are given as follows:

$$\text{Stage UC: } \sigma_1^c = E'_c \bar{\epsilon}_1 + \sigma_{ci}, \quad \bar{\epsilon}_1 \leq |\bar{\epsilon}_{ci}| \quad (1)$$

$$\text{Stage T1: } \sigma_1^c = E''_c (\bar{\epsilon}_1 + \bar{\epsilon}_{ci} - \bar{\epsilon}_{cx}), \quad |\bar{\epsilon}_{ci}| < \bar{\epsilon}_1 \leq (\bar{\epsilon}_{cr} - \bar{\epsilon}_{ci}) \quad (2)$$

$$\text{Stage T2: } \sigma_1^c = f_{cr} \left( \frac{\bar{\epsilon}_{cr}}{\bar{\epsilon}_1 + \bar{\epsilon}_{ci}} \right)^{0.5}, \quad \bar{\epsilon}_1 > (\bar{\epsilon}_{cr} - \bar{\epsilon}_{ci}) \quad (3)$$

The smeared (average) constitutive relationships of concrete compressive stress  $\sigma_2^c$  and the uniaxial compressive strain  $\bar{\epsilon}_2$  are given as follows:

$$\sigma_2^c = E_c' \bar{\varepsilon}_2, \quad \frac{\bar{\varepsilon}_2}{\zeta \varepsilon_0} \leq 0.5 \quad (4a)$$

or

$$\sigma_2^c = D \zeta f_c' \left[ 2 \left( \frac{\bar{\varepsilon}_2}{\zeta \varepsilon_0} \right) - \left( \frac{\bar{\varepsilon}_2}{\zeta \varepsilon_0} \right)^2 \right], \quad 0.5 < \frac{\bar{\varepsilon}_2}{\zeta \varepsilon_0} \leq 1 \quad (4b)$$

or

$$\sigma_2^c = D \zeta f_c' \left[ 1 - \left( \frac{\bar{\varepsilon}_2 / \zeta \varepsilon_0 - 1}{4 / \zeta - 1} \right)^2 \right], \quad \frac{\bar{\varepsilon}_2}{\zeta \varepsilon_0} > 1 \quad (4c)$$

where  $E_c'$  is the secant slope of the ascending parabolic compression curve of concrete given by (4b) between the initial point and the point corresponding to a compressive strain of 50% of the peak compressive strain.  $\zeta$  is the softening coefficient.

The softening coefficient in Eq. (4) can be determined as follows

$$\zeta = f(f_c') f(\bar{\varepsilon}_1) f(\beta) W_p \leq 0.9 \quad (5)$$

where

$$f(f_c') = \frac{5.8}{\sqrt{f_c'}} \leq 0.9 \quad (f_c' \text{ in MPa}) \quad (6)$$

$$f(\bar{\varepsilon}_1) = \frac{1}{\sqrt{1 + 400 \bar{\varepsilon}_1}} \quad (7)$$

$$f(\beta) = 1 - \frac{|\beta|}{24^\circ} \quad (8)$$

$$W_p = 1.15 + \frac{|\beta|(0.09|\beta| - 1)}{6} \quad (9)$$

and

$$\beta = \frac{1}{2} \tan^{-1} \left[ \frac{\gamma_{21}}{(\varepsilon_2 - \varepsilon_1)} \right] \quad (10)$$

During unloading and reloading stages the stress strain relationship of prestressed concrete is the same that of reinforced concrete (Fig. 3) and is given as follows:

$$\sigma^c = \sigma_i^c + E_{cc}(\bar{\varepsilon}_i - \bar{\varepsilon}) \quad (11)$$

where

$$E_{cc} = \frac{\sigma_i^c - \sigma_{i+1}^c}{\bar{\varepsilon}_i - \bar{\varepsilon}_{i+1}} \quad (12)$$

where  $(\sigma_i^c, \bar{\varepsilon}_i)$  and  $(\sigma_{i+1}^c, \bar{\varepsilon}_{i+1})$  are the stress-strains at the beginning and end of any loading or unloading stage in the stress strain relationship of concrete (Fig. 3).

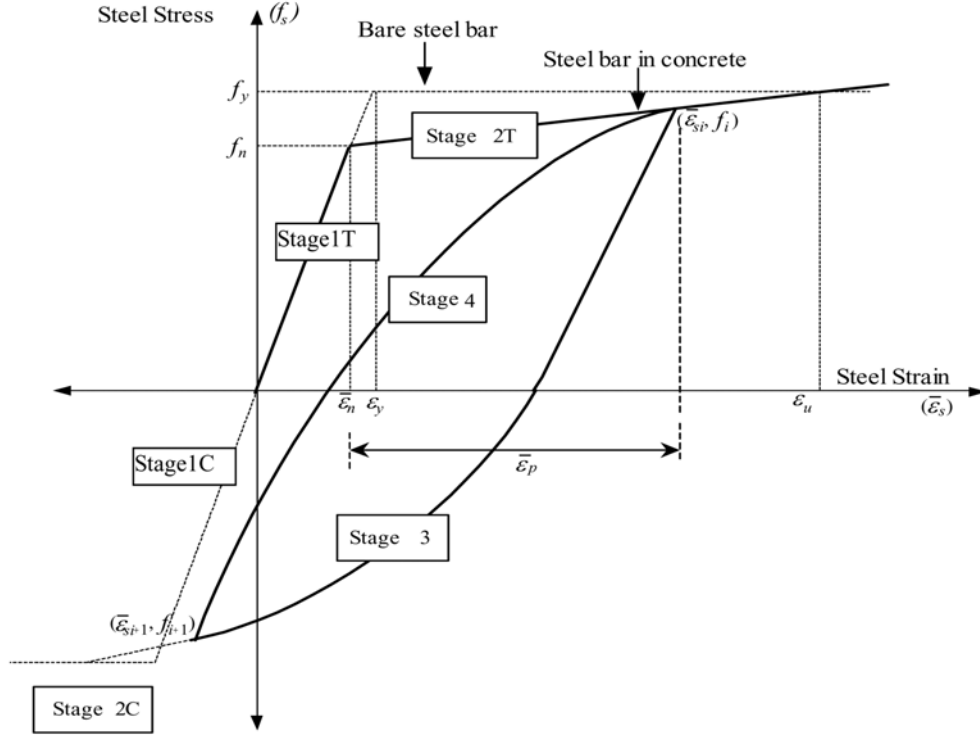


Fig. 4 Cyclic smeared stress strain bars of embedded mild steel bars

The equation relating the shear stress of concrete  $\tau_{21}^c$  and the shear strain  $\gamma_{21}$  is given by

$$\tau_{21}^c = \frac{\sigma_1^c - \sigma_2^c}{2(\varepsilon_1 - \varepsilon_2)} \gamma_{21} \quad (13)$$

## 2.2 Constitutive relationships of mild steel embedded in concrete

The smeared (average) tensile stress-strain relationships of mild steel embedded in concrete in the  $l-t$  coordinates (Fig. 4) are expressed as follows:

$$\text{Stage 1T: } f_s = E_s \bar{\varepsilon}_s, \quad \bar{\varepsilon}_s \leq \bar{\varepsilon}_n \quad (14)$$

$$\text{Stage 2T: } f_s = f_y \left[ (0.91 - 2B) + (0.02 + 0.25B) \frac{\bar{\varepsilon}_s}{\varepsilon_y} \right], \quad \bar{\varepsilon}_s > \bar{\varepsilon}_n \quad (15)$$

where

$$\bar{\varepsilon}_n = \varepsilon_y (0.93 - 2B) \quad (16)$$

and

$$B = \frac{1}{\rho} \left( \frac{f_{cr}}{f_y} \right)^{1.5} \quad (17)$$

The smeared (average) constitutive relationships of embedded mild steel in compression are given as follows:

$$\text{Stage 1C: } f_s = E_s \bar{\varepsilon}_s, \quad \bar{\varepsilon}_s \leq \bar{\varepsilon}_n \quad (17)$$

$$\text{Stage 2C: } f_s = -f_y, \quad \bar{\varepsilon}_s > \bar{\varepsilon}_n \quad (18)$$

During unloading and reloading stages the stress strain relationship is given as follows:

$$\bar{\varepsilon}_s - \bar{\varepsilon}_{si} = \frac{f_s - f_i}{E_s} \left[ 1 + A^{-R} \left| \frac{f_s - f_i}{f_y} \right|^{R-1} \right] \quad (19)$$

where

$$A = 1.9 k_p^{-0.1} \quad (20)$$

$$R = 10 k_p^{-0.2} \quad (21)$$

$$k_p = \frac{\bar{\varepsilon}_p}{\bar{\varepsilon}_n} \quad (22)$$

In the above equations,  $l$  replaces  $s$  in the subscript of symbols for the longitudinal steel, and  $t$  replaces  $s$  for the transverse steel. Quantities with subscript  $i$  indicate conditions at the beginning of unloading or reloading step.

### 2.3 Constitutive relationships of prestressing tendons embedded in concrete

The smeared (average) stress-strain relationships of prestressing tendons embedded in concrete are given as follows:

$$f_{ps} = E_{ps} \bar{\varepsilon}_s, \quad \bar{\varepsilon}_s \leq \frac{0.7 f_{pu}}{E_{ps}} \quad (23a)$$

or

$$f_{ps} = \frac{E_{ps}'' \varepsilon_s}{\left[ 1 + \left( \frac{E_{ps}'' \bar{\varepsilon}_s}{f_{pu}'} \right)^5 \right]^{\frac{1}{5}}}, \quad \bar{\varepsilon}_s \geq \frac{0.7 f_{pu}}{E_{ps}} \quad (23b)$$

where

$E_{ps}$  = elastic modulus of prestressing tendons taken as 200 Gpa (29,000 ksi),

$f_{pu}$  = ultimate strength of prestressing tendons taken as 1862 MPa (270 ksi),

$E_{ps}''$  = modulus of prestressing tendons, used in plastic region (22b), taken as 209 GPa (30,345 ksi), and

$f_{pu}'$  = revised strength of prestressing tendons taken as 1793 MPa (260 ksi).

In the above equations,  $lp$  replaces  $ps$  in the subscript of symbols for the longitudinal tendons, and  $tp$  replaces  $ps$  for the transverse tendons.

The cyclic behavior of mild steel can be extended to prestressing tendons. Hence during unloading and reloading stages, the stress strain relationship of prestressing tendons is the same as that of mild steel, as given by Eqs. (19) through (22).

### 3. Element scale

#### 3.1 Modeling cracked reinforced concrete

In a smeared crack model, cracked reinforced concrete is considered to remain in continuum. The material properties are characterized by a set of smeared (or average) stress-strain relationships for concrete and steel established directly from full-scale element tests subject to biaxial loading (Vecchio and Collins 1981, 1986, Belarbi and Hsu 1994, 1995, Pang and Hsu 1995, Hsu and Zhang 1997). These average stress-strain relationships account for local bond slipping. This type of modeling has also been done in Japan (Noguchi and Inoue 1983, Noguchi 1992, Shin *et al.* 1992, Izumo *et al.* 1992, Inoue and Suzuki 1992), in Europe (Rots *et al.* 1985, de Borst and Nauta 1985) and in North America (Stevens *et al.* 1987, Vecchio and Collins 1988, Vecchio 1989, 1990, Polak and Vecchio 1993, Selby and Vecchio 1993, Ayoub and Filippou 1998). An important advantage of using the averaging concept in tension stiffening (Hsu and Zhang 1996) is that the tensile stress-strain relationship of concrete becomes mesh independent.

#### 3.2 Development of elements from constitutive laws

The constitutive laws of concrete, mild steel and prestressing tendons discussed in Section 2 are combined with the equilibrium and compatibility equations to form a tangent stiffness matrix  $[D]$  for a reinforced/prestressed concrete element.  $[D]$  is formulated as:

$$[D] = \frac{d \begin{Bmatrix} \sigma_x \\ \sigma_y \\ \tau_{xy} \end{Bmatrix}}{d \begin{Bmatrix} \varepsilon_x \\ \varepsilon_y \\ \frac{1}{2} \gamma_{xy} \end{Bmatrix}} \quad (24)$$

Using incremental stresses, the equilibrium equations that relate the applied incremental stresses in the  $x$ - $y$  coordinate ( $\sigma_1^c$ ,  $\sigma_2^c$  and  $\tau_{12}^c$ ) to the internal incremental concrete stresses ( $\sigma_x$ ,  $\sigma_y$  and  $\tau_{xy}$ ) in the principal stress directions, and the incremental steel bar stresses ( $f_{si}$ ) in the bar directions is given by:

$$d \begin{Bmatrix} \sigma_x \\ \sigma_y \\ \tau_{xy} \end{Bmatrix} = [T(-\theta_1)] d \begin{Bmatrix} \sigma_1^c \\ \sigma_2^c \\ \tau_{12}^c \end{Bmatrix} + \sum_i [T(-\theta_{si})] d \begin{Bmatrix} \rho_{si} f_{si} \\ 0 \\ 0 \end{Bmatrix} \quad (25)$$

where  $[T(-\theta_1)]$  and  $[T(-\theta_{s,i})]$  are the transformation matrices from the 1-2 coordinate and the  $x_{s,i}$ - $y_{s,i}$  coordinate to the  $x$ - $y$  coordinate, respectively. A typical transformation matrix between two coordinates at an angle  $\alpha$  apart,  $[T(\alpha)]$  is given by:

$$[T(\alpha)] = \begin{bmatrix} c^2 & s^2 & 2sc \\ s^2 & c^2 & -2sc \\ -sc & sc & c^2 - s^2 \end{bmatrix} \quad (26)$$

where  $c = \cos(\alpha)$  and  $s = \sin(\alpha)$ .

$\rho_{s,i}$  is the steel ratio in the “ $i^{\text{th}}$ ” direction.

The compatibility equations define the relationships between the incremental steel strains ( $d\varepsilon_{s,i}$ ) in the  $x_{s,i}$ - $y_{s,i}$  coordinate and the incremental concrete strains ( $d\varepsilon_1, d\varepsilon_2$  and  $\frac{1}{2}d\gamma_{12}$ ) in the 1-2 coordinate. It is expressed by Eq. (27):

$$d \begin{Bmatrix} \varepsilon_{s,i} \\ \varepsilon_{s,i'} \\ \frac{1}{2}\gamma_{s,i} \end{Bmatrix} = [T(\theta_{s,i}-\theta_1)] d \begin{Bmatrix} \varepsilon_1 \\ \varepsilon_2 \\ \frac{1}{2}\gamma_{12} \end{Bmatrix} \quad (27)$$

The incremental strains transformed from the  $x$ - $y$  coordinate to the 1-2 coordinate using the transformation matrix are expressed as follows:

$$d \begin{Bmatrix} \varepsilon_1 \\ \varepsilon_2 \\ \frac{1}{2}\gamma_{12} \end{Bmatrix} = [T(\theta_1)] d \begin{Bmatrix} \varepsilon_x \\ \varepsilon_y \\ \frac{1}{2}\gamma_{xy} \end{Bmatrix} \quad (28)$$

It is noted that the incremental steel strains ( $d\varepsilon_{s,i}$ ) and incremental concrete strains ( $d\varepsilon_1, d\varepsilon_2$ ) in Eq. (28) are biaxial strains, which take into account the Poisson effect using the Hsu/Zhu ratios of cracked reinforced concrete (Zhu and Hsu 2002).

Using the Hsu/Zhu ratios ( $\nu_{12}, \nu_{21}$ ), the incremental biaxial strains of concrete ( $d\varepsilon_1, d\varepsilon_2$ ) in Eq. (28) are converted into the incremental uniaxial strains of concrete ( $d\bar{\varepsilon}_1, d\bar{\varepsilon}_2$ ) as follows:

$$d \begin{Bmatrix} \bar{\varepsilon}_1 \\ \bar{\varepsilon}_2 \\ \frac{1}{2}\gamma_{12} \end{Bmatrix} = [V] \cdot d \begin{Bmatrix} \varepsilon_1 \\ \varepsilon_2 \\ \frac{1}{2}\gamma_{12} \end{Bmatrix} \quad (29)$$

where

$$[V] = \begin{bmatrix} \frac{1}{1 - \nu_{12} \nu_{21}} & \frac{\nu_{12}}{1 - \nu_{12} \nu_{21}} & 0 \\ \frac{\nu_{21}}{1 - \nu_{12} \nu_{21}} & \frac{1}{1 - \nu_{12} \nu_{21}} & 0 \\ 0 & 0 & 1 \end{bmatrix} \quad (30)$$

The incremental uniaxial strains of concrete ( $d\bar{\varepsilon}_1, d\bar{\varepsilon}_2$ ) can then be transformed to the incremental uniaxial strain of steel ( $d\bar{\varepsilon}_{si}$ ) as follows:

$$d \begin{Bmatrix} \bar{\varepsilon}_{si} \\ \bar{\varepsilon}_{s'i'} \\ \frac{1}{2} \gamma_{si} \end{Bmatrix} = [T(\theta_{si} - \theta_1)] d \begin{Bmatrix} \bar{\varepsilon}_1 \\ \bar{\varepsilon}_2 \\ \frac{1}{2} \gamma_{12} \end{Bmatrix} \quad (31)$$

Once the incremental uniaxial strains of concrete ( $d\bar{\varepsilon}_1, d\bar{\varepsilon}_2$ ) and steel ( $d\bar{\varepsilon}_{si}$ ) are obtained using Eqs. (29) through (31), the incremental stresses of concrete ( $d\sigma_1^c, d\sigma_2^c, d\tau_{12}^c$ ) and steel ( $df_{si}$ ) in Eq. (25) can be determined using the uniaxial tangential constitutive matrices of concrete,  $[D_c]$  and steel,  $[D_{si}]$  as shown below:

$$d \begin{Bmatrix} \sigma_1^c \\ \sigma_2^c \\ \tau_{12}^c \end{Bmatrix} = [D_c] d \begin{Bmatrix} \bar{\varepsilon}_1 \\ \bar{\varepsilon}_2 \\ \frac{1}{2} \gamma_{12} \end{Bmatrix} \quad (32)$$

where

$$[D_c] = \begin{bmatrix} \overset{=}{E}_1^c & \frac{\partial \sigma_1^c}{\partial \bar{\varepsilon}_2} & 0 \\ \frac{\partial \sigma_2^c}{\partial \bar{\varepsilon}_1} & \overset{=}{E}_2^c & 0 \\ 0 & 0 & G_{12}^c \end{bmatrix} \quad (33)$$

where  $\overset{=}{E}_1^c$  and  $\overset{=}{E}_2^c$  are the tangential stiffness of uniaxial moduli of concrete in the 1 and 2 directions evaluated at a stress/strain state; off-diagonal terms  $\frac{\partial \sigma_1^c}{\partial \bar{\varepsilon}_2}$  and  $\frac{\partial \sigma_2^c}{\partial \bar{\varepsilon}_1}$  can be obtained by using the uniaxial constitutive relationships and taking into account the states of the concrete stresses and uniaxial strains in the 1-2 directions (Zhong 2005).  $G_{12}^c$  is the shear modulus of concrete.

$$d \begin{Bmatrix} \rho_{si} f_{si} \\ 0 \\ 0 \end{Bmatrix} = [D_{si}] d \begin{Bmatrix} \bar{\varepsilon}_{si} \\ \bar{\varepsilon}_{si'} \\ \frac{1}{2} \gamma_{si} \end{Bmatrix} \quad (34)$$

where

$$[D_{si}] = \begin{bmatrix} \rho_{si} \cdot \bar{E}_{si} & 0 & 0 \\ 0 & 0 & 0 \\ 0 & 0 & 0 \end{bmatrix} \quad (35)$$

where  $\bar{E}_{si}$  is the uniaxial tangential modulus for the rebars, as determined for a particular stress/strain state.

Substituting Eq. (24) to the left hand side (LHS) of Eq. (25) and Eqs. (26) through (35) to the RHS of Eq. (25),  $[D]$  is evaluated as follows:

$$[D] = [T(-\theta_1)][D_c][V][T(\theta_1)] + \sum_i [T(-\theta_{si})][D_{si}][T(\theta_{si} - \theta_1)][V][T(\theta_1)] \quad (36)$$

## 4. Structure scale

### 4.1 Analysis procedure

An iterative tangent-stiffness procedure under incremental load or displacement is developed to perform nonlinear analysis for reinforced concrete structures. A flow chart of the procedure is shown in Fig. 5. Throughout the procedure, the material stiffness matrix  $[D]$  is determined first using the materials constitutive laws described in Section 2. The element stiffness matrix  $[k]$  is calculated using the material stiffness matrix discussed in Section 3 with the shape function matrix of the element. The incremental element force vector  $\Delta f$  is obtained from the loading applied on the structure. Then the global stiffness matrix  $[K]$  and incremental global force vector  $\Delta F$  are assembled. In each iteration, the material stiffness matrix  $[D]$ , the element stiffness matrix  $[k]$ , and the global stiffness matrix  $[K]$  are iteratively refined until convergence is achieved. It is noted that an additional iterative loop is defined to obtain the material stiffness matrix  $[D]$  because the principal stress direction  $\theta_1$  is an unknown value before  $[D]$  is found.

### 4.2 Opensees

OpenSees stands for Open System for Earthquake Engineering Simulation (Fenves (2005)). OpenSees has been developed in the Pacific Earthquake Engineering Research Center (PEER) and is an object-oriented framework for simulation applications in earthquake engineering using finite element methods. An object-oriented framework is a set of cooperating classes that can be used to

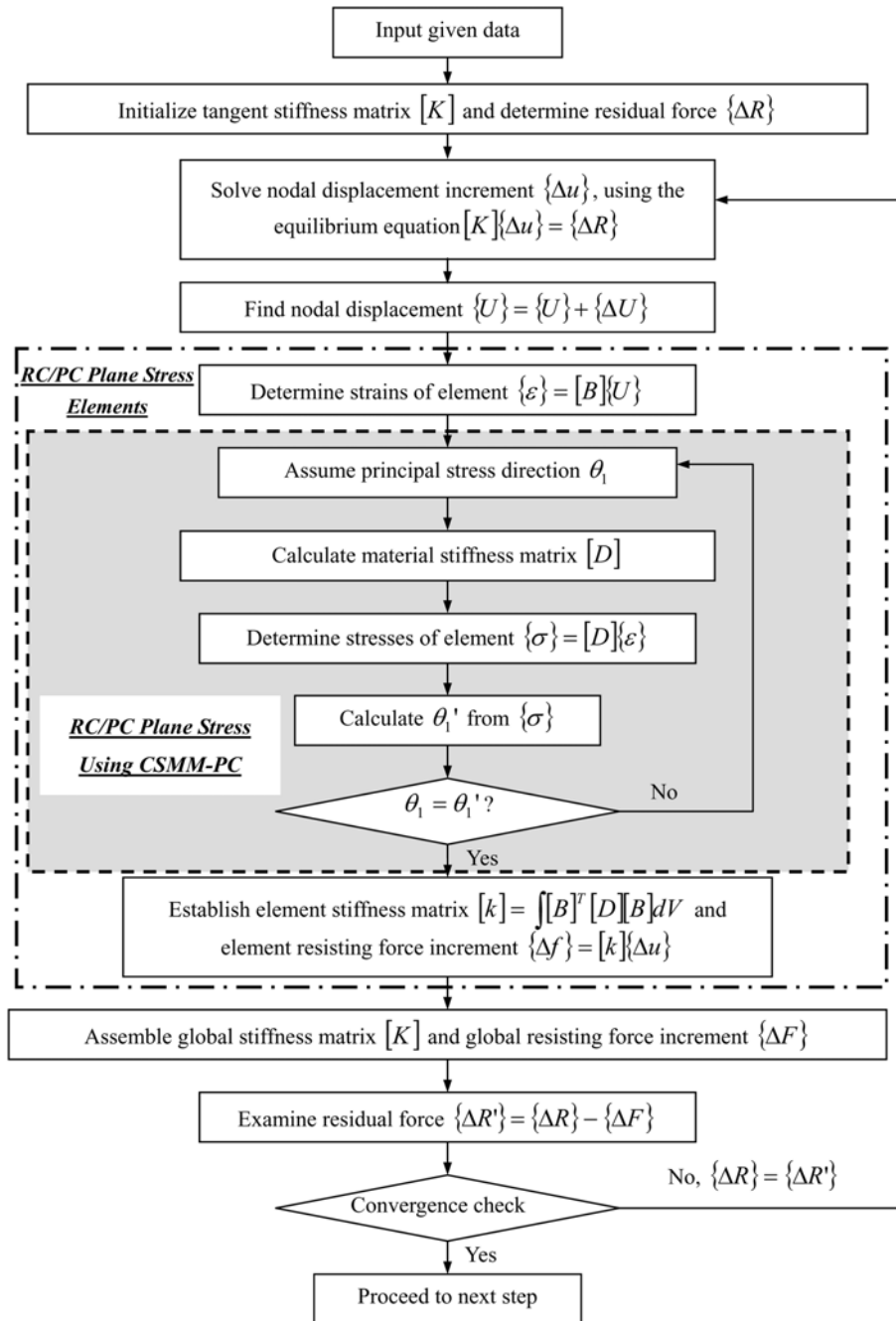


Fig. 5 Nonlinear analysis algorithm

generate software for a specific class of problem, such as finite element analysis. The framework dictates overall program structure by defining the abstract classes, their responsibilities, and how these classes interact. OpenSees is a communication mechanism for exchanging and building upon

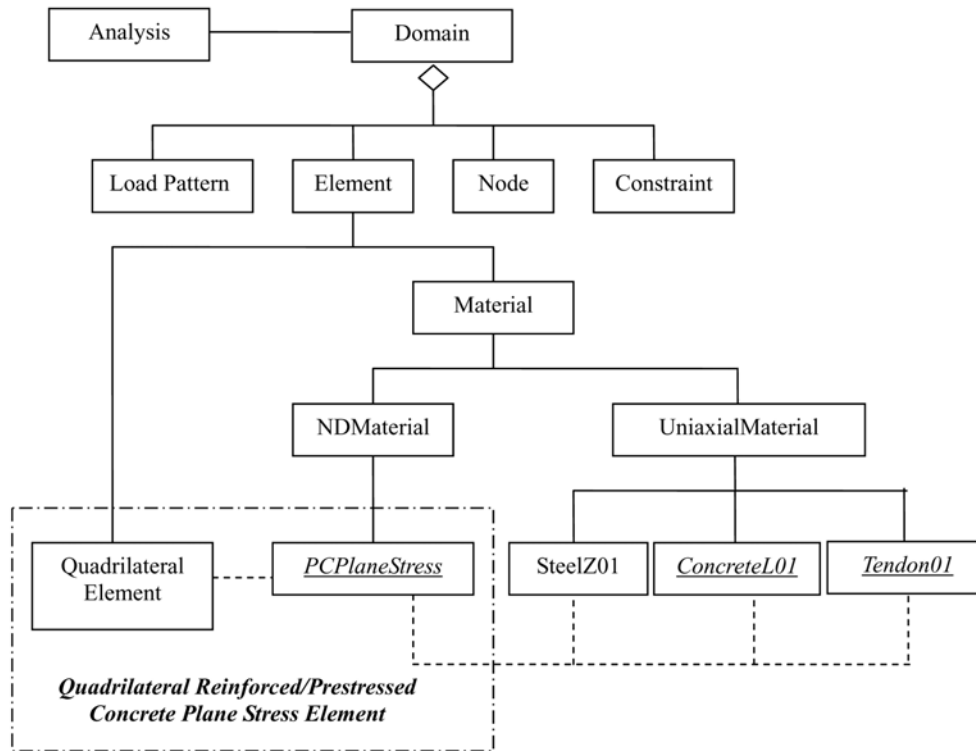


Fig. 6 Implementation of CSMM into OpenSeeS

research accomplishments, and has the potential for a community code for earthquake engineering because it is an open source.

In order to implement the CSMM for RC into OpenSees, three new material modules, namely SteelZ01, ConcreteZ01 and RCPlaneStress are developed. The integration of SteelZ01, ConcreteZ01, RCPlaneStress and existing libraries of OpenSees are presented in Fig. 6. SteelZ01 and ConcreteZ01 are the uniaxial material modules, in which the uniaxial constitutive relationships of steel and concrete specified in the CSMM are defined. The RCPlaneStress is implemented with the quadrilateral element to represent the four node reinforced concrete membrane elements. The uniaxial materials of SteelZ01 and ConcreteZ01 are related with material RCPlaneStress to determine the material stiffness matrix of membrane reinforced concrete in RCPlaneStress. Using the OpenSees as the finite element framework, a nonlinear finite element program titled Simulation of Reinforced Concrete Structures (SRCS) was developed for the simulation of reinforced concrete structures subjected to monotonic and reversed cyclic loading. It should be noted that SRCS is being presently extended to include prestressed concrete also. The constitutive laws of prestressing tendons and concrete under initial prestressing (as described in Section 2 of this paper) are being implemented into OpenSees for this purpose.

## 5. Validation

SRCS has been validated by conducting analysis of tested RC structures and comparing the

analytical results with the test results. The validation studies have been conducted with experimental results of framed shear wall tests under reversed loading as well as under shake table excitation. The results of this study are reported in Sections 5.1 and 5.2 respectively.

### 5.1 Framed walls under reversed cyclic loading

Tests on 1/3-scale framed shear walls, subjected to a constant axial load at the top of each column and a reversed cyclic load at the top beam, were performed at the University of Houston (Gao (1999)). The wall dimensions were 914.4 mm by 914.4 mm with a thickness of 76.2 mm. The cross-section of the boundary columns was 152.4 mm square. Fig. 7 demonstrates the details of dimensions and reinforcement of the specimens. The bottom left and right corners of the specimen were supported by a hinge and a roller, respectively (Fig. 8).

Finite element analyses were conducted on these specimens. The specimens were modeled by the finite element mesh shown in Fig. 8. The wall panel was defined by nine RCPlaneStress quadrilateral elements. Each of the boundary columns and beams were modeled by three NonlinearBeamColumn elements (Taucer *et al.* 1991). In the beginning of the analysis, axial loads were applied as vertical nodal loads to the columns using load control. After that, axial loads were kept constant and reversed cyclic horizontal loads were applied by a predetermined displacement control scheme. The nodal displacement and corresponding horizontal forces were recorded at each converged displacement step, and the stress and strain of the elements were also monitored.

The analytical results of the shear force-drift relationships of two shear walls are illustrated by the dashed hysteretic loops in Fig. 9. These dotted loops are compared to the solid loops, representing the experimental results. It can be seen that good agreements were obtained for the primary backbone curves, the initial stiffness, the yield point, the ultimate strength, and the failure state in the descending branch. The hysteretic behavior provided accurate measurements of the pinching

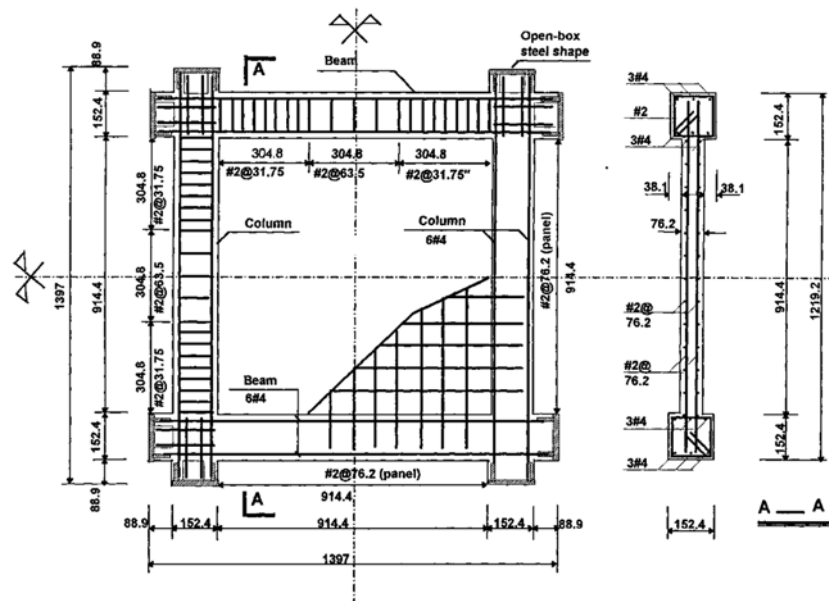


Fig. 7 Dimensions and steel arrangement of specimen (Unit: mm, 1 mm = 0.0394 in)

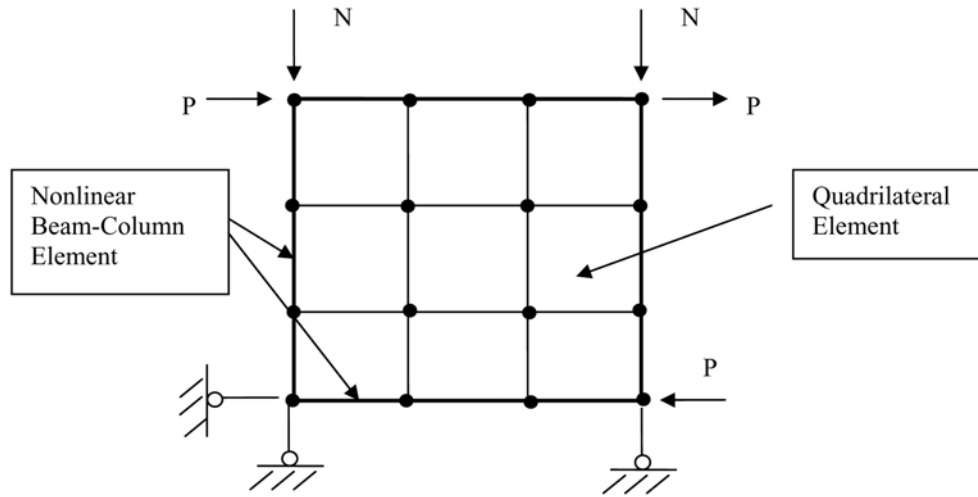


Fig. 8 Finite element modeling of walls

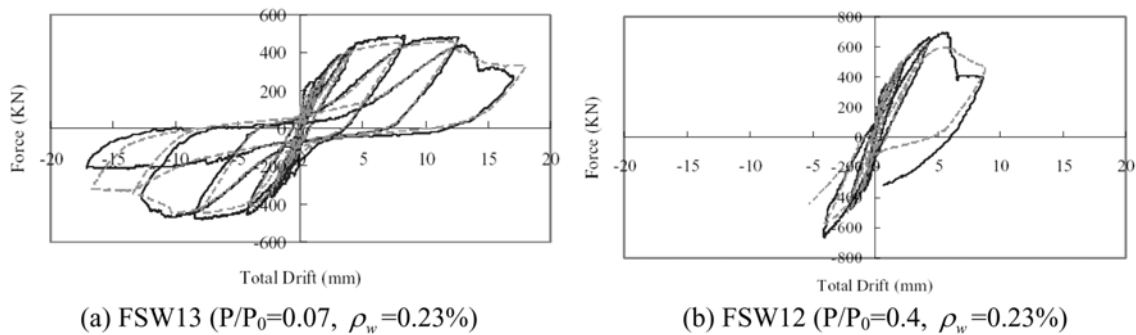
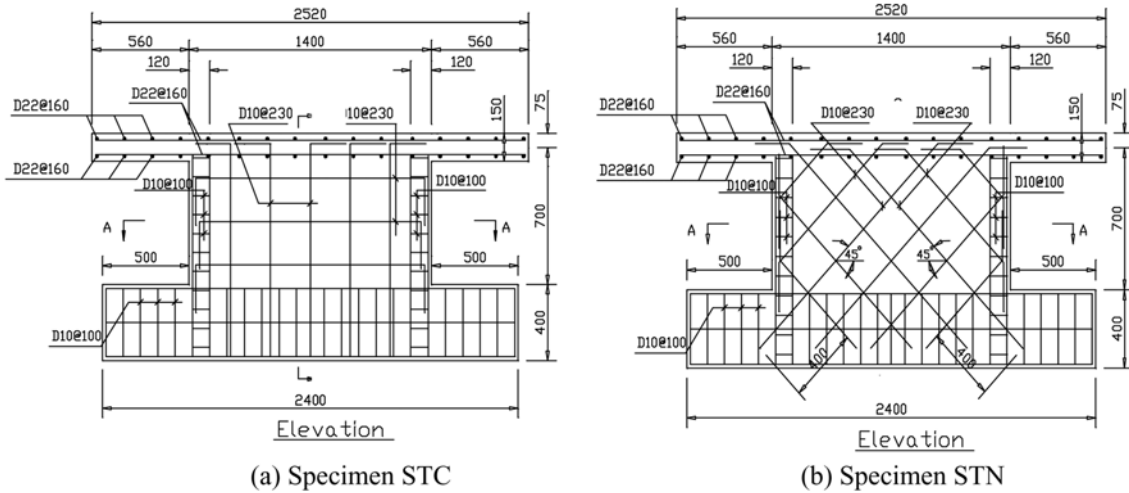


Fig. 9 Shear force - drift displacement of specimens

effect, the residual displacements, the ductility and the energy dissipation capacity in all specimens. Even the failure modes can be predicted by the CSMM-based finite element program. In specimen FSW13 steel bars in the walls yielded significantly prior to the concrete crushing, resulting in long yield plateaus. In contrast, in specimen FSW12 the concrete crushed right after the steel yielded, which caused an abrupt drop of the shear force in the descending branch. The program was able to capture the brittle failure behavior of these specimens.

### 5.2 Framed walls under shake table excitation

Two low-rise shear walls having the same dimensions of 625 mm in height, 1400 mm in length, and 60 mm in thickness were tested on a shake table. The two specimens named STC and STN were designed identically with the exception of the steel grid orientation in the walls. The specimen STC was a conventional shear wall with the steel grid in the horizontal and vertical directions (Fig. 10(a)). The specimen STN had a new steel grid orientation in the wall panel. The wall reinforcements in the specimen were oriented at 45 degrees to the horizontal (Fig. 10(b)). The shear



(a) Specimen STC

(b) Specimen STN

Fig. 10 Dimension and steel arrangement of specimens

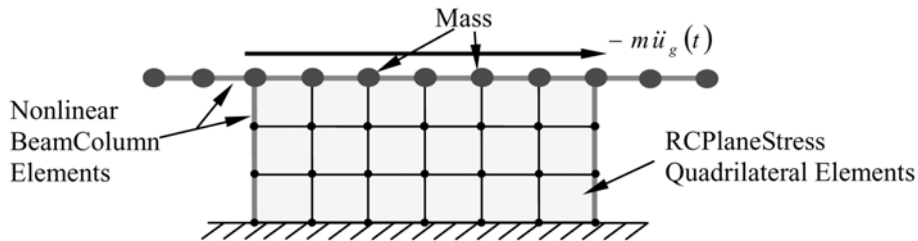


Fig. 11 Finite element mesh of specimen

walls were subjected to seismic excitations on a shake table, which is located at the National Center for Research on Earthquake Engineering (NCREE), Taipei, Taiwan. The *tcu078Eji* seismogram of the 1999 Taiwan earthquake was used as the ground motion acceleration for the shake table. In each test run, a scale factor was applied to the input ground motion acceleration such that the peak ground acceleration (PGA) would reach the predetermined value.

As illustrated in Fig. 11, the finite element mesh of the structure was divided into three zones: the web panel, the boundary columns, and the top slab. The wall panel was modeled using 18 RCPlaneStress quadrilateral elements. Each of the two boundary columns was modeled using 3 NonlinearBeamColumn elements, and the top slab was modeled using 10 NonlinearBeamColumn elements. Only one type of RCPlaneStress Quadrilateral elements was defined in the finite element model for each specimen due to the fact that the steel grid orientation and spacing was the same for all 18 elements in the wall panel. The steel grid orientation in the RCPlaneStress Quadrilateral elements of specimen STN was defined at 45 degrees and 135 degrees with respect to the horizontal. In contrast, the steel grid orientation in the RCPlaneStress Quadrilateral elements of specimen STC was defined in the horizontal and vertical directions.

The calculated drift and time history of specimens STC and STN for the fifth run are presented in Figs. 12 (a) and (b), respectively. Also, the analytical hysteretic loops (inertial force  $-m\ddot{y}$  vs drift  $u$ ) of specimens STC and STN for the fifth runs are shown in Figs. 12(a) and (b), respectively. The

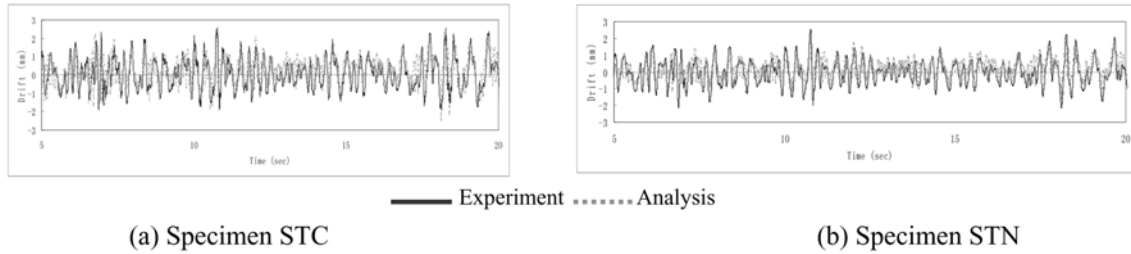


Fig. 12 Measured and computed drift time history of specimens in fifth run

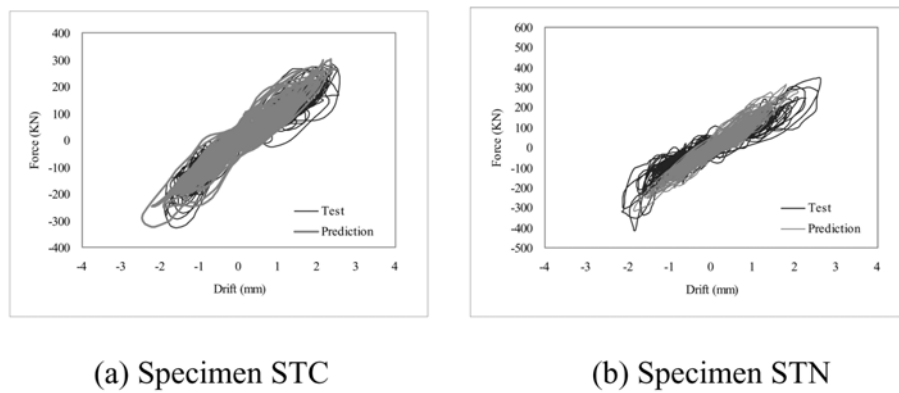


Fig. 13 Comparison of measured and computed hysteretic response of specimens in fifth run

computed drift and time histories show good agreements with the measured responses for both specimens. Figs. 13 (a) and (b) show that good agreements are achieved between the analytical and experimental hysteretic responses in terms of amplitude, stiffness and hysteretic behavior under the multi cycles of the responses. The results also show that the damping ratios used in the analyses were appropriate to take into account the different damage levels of the structure. Results showing good agreements between tests and analysis were also obtained for other test runs of the specimens.

### 5.3 Post tensioned precast column under reversed cyclic loading

A full-scale post tensioned precast hollow bridge column has been tested at the State University of New York, Buffalo (Ou (2002)). The column has a dimension of 860 mm  $\times$  860 mm with 200 mm thick walls. The height of the column is 4050 mm. Fig. 14 demonstrates the details of dimensions and reinforcement of the specimen. The column has been post tensioned with a prestressing force of 1042 kN using the prestressing tendons running through the center of the specimen.

Finite element analysis of the specimen was conducted using SCS. The specimens were modeled by the finite element mesh shown in Fig. 15. The wall panel was defined by sixteen PCPlaneStress quadrilateral elements. Each of the boundary columns and beams were modeled by eight NonlinearBeamColumn elements. In the beginning of the analysis, axial loads were applied as vertical nodal loads to the columns using load control. The prestressing load was also applied as

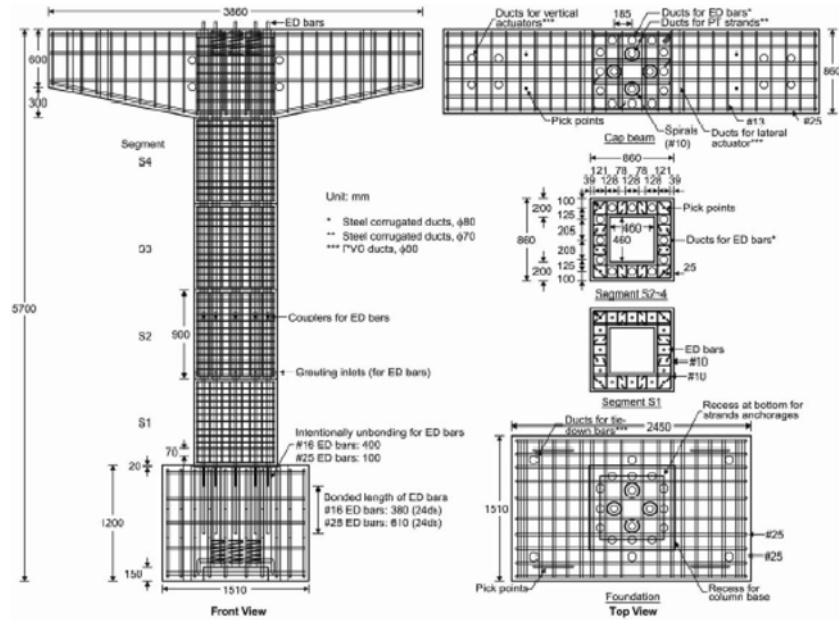


Fig. 14 Design details of precast column specimen

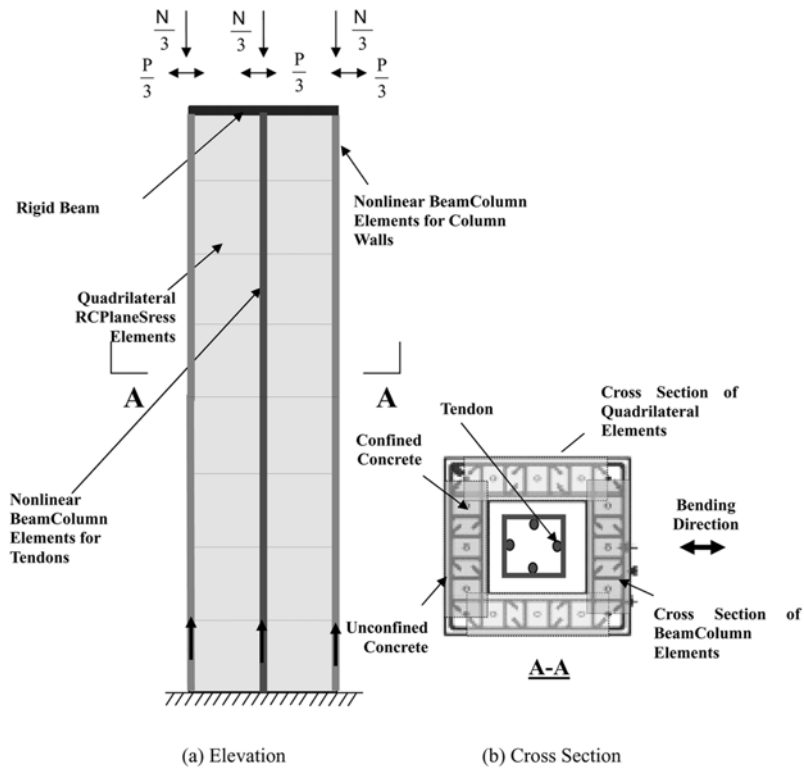


Fig. 15 Finite element mesh of column specimen

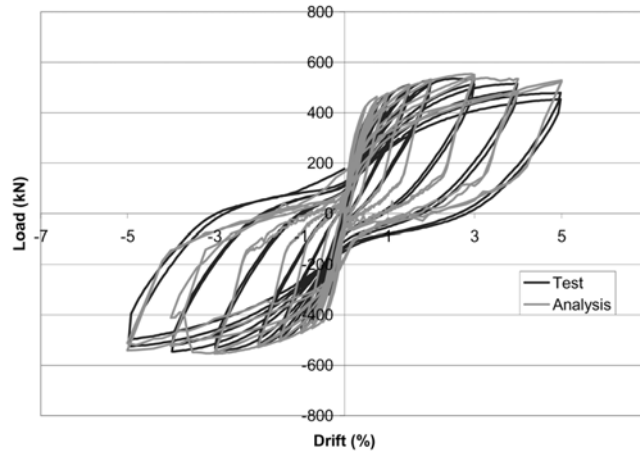


Fig. 16 Experimental and analytical load drift diagram of column specimen

nodal loads at the top and bottom of the column. After that, the axial and prestressing loads were kept constant and reversed cyclic horizontal loads were applied by a predetermined displacement control scheme. The nodal displacements and corresponding horizontal forces were recorded at each converged displacement step, and the stress and strain of the elements were also monitored.

The analytical results of the load-drift relationships of the column specimen are illustrated by the light-dotted hysteretic loops in Fig. 16. These light-dotted loops are compared to the dark loops, representing the experimental results. It can be seen that good agreements were obtained for the primary backbone curves, the initial stiffness, the yield point, the ultimate strength, and the failure state in the descending branch. The hysteretic behavior provided accurate measurements of the residual displacements, the ductility and the energy dissipation capacity of the specimen.

## 6. Conclusions

Multiscale modeling of reinforced/prestressed concrete thin-walled structures is presented in this paper. In material scale, all related constitutive models are determined by testing full scale reinforced as well as prestressed concrete panels using the Universal Panel Tester available at the University of Houston. The development of RC/PC plane stress elements is discussed in this paper in the element scale. Using OpenSees as a framework, a finite element program for the structural scale analysis of RC/PC thin-walled structures is developed. The developed finite element program was validated by three series of tests on reinforced concrete wall structures subjected to reversed cyclic loading and shake table excitations as well as a precast prestressed concrete column subjected to reversed cyclic loading. The predicted results agree well with the experimental data of all the walls under reversed cyclic loading, two walls under shake table excitations and a precast prestressed concrete column under reversed cyclic loading. However it should be noted that the CSMM is a smeared crack model, the finite element analysis of reinforced/prestressed concrete structures using SCS is very successful for structures with cracks uniformly distributed, which undergo global failures. The current SCS may not accurately predict the failure modes of RC/PC structures which fail in local regions.

## References

- Ayoub, A. and Filippou, F.C. (1998), "Nonlinear finite-element analysis of RC shear panels and walls", *J. Struct. Eng.*, March, 298-308.
- Belarbi, A. and Hsu, T.T.C. (1994), "Constitutive laws of concrete in tension and reinforcing bars stiffened by concrete", *Struct. J. American Concrete Institute*, **91**(4), 465-474.
- Belarbi, A. and Hsu, T.T.C. (1995), "Constitutive laws of softened concrete in biaxial tension-compression", *Struct. J. American Concrete Institute*, **92**(5), 562-573.
- De Borst, R. and Nauta, P. (1985), "Non-orthogonal cracks in a smeared finite element model", *Eng. Comput.*, **2**, 23-46.
- Fenves, G.L. (2005), *Annual workshop on Open System for Earthquake Engineering Simulation*, Pacific Earthquake Engineering Research Center, UC Berkeley.
- Gao, X.D. (1999), "Framed shear walls under cyclic loading", Ph. D. Dissertation, Department of Civil and Environmental Engineering, University of Houston, Houston, TX.
- Hsu, T.T.C. (1993), *Unified Theory of Reinforced Concrete*, Boca Raton: CRC Press Inc.
- Hsu, T.T.C. and Zhang, L.X. (1996), "Tension stiffening in reinforced concrete membrane elements", *Struct. J. American Concrete Institute*, **93**(1), 108-115.
- Hsu, T.T.C. and Zhu, R.R.H. (2002), "Softened membrane model for reinforced concrete elements in shear", *Struct. J. American Concrete Institute*, **99**(4), 460-469.
- Hsu, T.T.C. and Mansour, M.Y. (2005), "Stiffness, ductility, and energy dissipation of RC elements under cyclic shear", *Earthquake Spectra*, EERI, **21**(4), 1093-1112.
- Izumo, J., Shin, H., Maekawa, K. and Okamura, H. (1992), "An analytical model for RC panels subjected to in-plane stresses, concrete shear in earthquake", *Proceedings of the International Workshop on Concrete Shear in Earthquake*, Jan. 14-16, 1991, Houston, Elsevier Science Publishers, Inc., London-New York, 206-215.
- Inoue, N. and Suzuki, N. (1992), "Microscopic and macroscopic analysis of reinforced concrete framed shear walls, concrete shear in earthquake", *Proceedings of the International Workshop on Concrete Shear in Earthquake*, Jan. 14-16, 1991, Houston, Elsevier Science Publishers, Inc., London-New York, 333-342.
- Mansour, M. (2001), "Behavior of reinforced concrete membrane elements under cyclic shear: Experiments to theory", Ph. D. Dissertation, Department of Civil and Environmental Engineering, University of Houston, Houston, TX.
- Mansour, M. and Hsu, T.T.C. (2005a), "Behavior of reinforced concrete elements under cyclic shear: Part 1 - experiments", *J. Struct. Eng., ASCE*, **131**(1), 44-53.
- Mansour, M. and Hsu, T.T.C. (2005b), "Behavior of reinforced concrete elements under cyclic shear: Part 2 - theoretical model", *J. Struct. Eng., ASCE*, **131**(1), 54-65.
- Mo, Y.L., Zhong, J. and Hsu, T.T.C. (2008), "Seismic simulation of RC wall-type structures", accepted for publication in *Engineering Structures*.
- Noguchi, H. and Inoue, N. (1983), "Analytical techniques of shear in reinforced concrete structures by finite element method", *Proceedings, JCI Colloquium on Shear analysis of RC Structures*, Japan Concrete Institute (C4E) Sept., 57-96.
- Noguchi, H. (1992), "State-of-the-art of theoretical studies on membrane shear behavior in Japan, Concrete Shear in Earthquake", *Proceedings of the International Workshop on Concrete Shear in Earthquake*, Jan. 14-16, 1991, Houston, Elsevier Science Publishers, Inc., London-New York, Jan. 1992, 196-205.
- Ou, Y.C. (2002), "Precast segmental post-tensioned concrete bridge columns for seismic regions", Ph.D. Dissertation, Department of Civil, Structural, and Environmental Engineering, State University of New York, Buffalo, NY.
- Pang, X.B. and Hsu, T.T.C. (1995), "Behavior of reinforced concrete membrane elements in shear", *Struct. J. American Concrete Institute*, **92**(6), 665-679.
- Pang, X.B. and Hsu, T.T.C. (1996), "Fixed-angle softened-truss model for reinforced concrete", *Struct. J. American Concrete Institute*, **93**(2), 197-207.
- Polak, M.A. and Vecchio, F.J. (1993), "Nonlinear analysis of reinforced concrete shells", *J. Struct. Eng., ASCE*, **116**(3), 730-750.
- Rots, J.G., Nauta, P., Kusters, G.M.A. and Blaawendraad, J. (1985), "Smeared crack approach and fracture

- localization in concrete”, *Heron*, **30**(1), 1-48.
- Selby, R.G. and Vecchio, F.J. (1993), “Three dimensional constitutive relations for reinforced concrete”, Report No. 93-02, Dept. of Civil Engineering, University of Toronto, 147 pages.
- Shin, H., Maekawa, K. and Okamura, H. (1992), “Analytical models for reinforced concrete shear walls under reversed cyclic loading, concrete shear in earthquake”, *Proceedings of the International Workshop on Concrete Shear in Earthquake*, Jan. 14-16, 1991, Houston, Elsevier Science Publishers, Inc., London-New York, Jan., 289-298.
- Stevens, N.J., Uzumeri, S.M. and Collins, M.P. (1987), “Analytical modeling of reinforced concrete subjected to monotonic and reversed cyclic loadings”, Publication No. 87-1, Dept. of Civil Engineering, University of Toronto, Toronto, Canada.
- Taucer, F.F., Spacone, E. and Filippou, F.C. (1991), “A fiber beam-column element for seismic response analysis of reinforced concrete structures”, Report No. UCB/EERC-91/17, EERC, UC Berkeley.
- Vecchio, F. and Collins, M.P. (1981), “Stress-strain characteristic of reinforced concrete in pure shear”, *IABSE Colloquium, Advanced Mechanics of Reinforced Concrete*, Delft, Final Report, International Association of Bridge and Structural Engineering, Zurich, Switzerland, 221-225.
- Vecchio, F.J. and Collins, M.P. (1986), “The modified compression field theory for reinforced concrete elements subjected to shear”, *ACI J.*, **83**(2), 219-231.
- Vecchio, F.J. and Collins, M.P. (1988), “Predicting the response of reinforced concrete beams subjected to shear using modified compression field theory”, *Struct. J. American Concrete Institute*, **85**, 258-267.
- Vecchio, F.J. (1989), “Nonlinear finite element analysis of reinforced concrete membranes”, *Struct. J. American Concrete Institute*, **86**(1), 26-35.
- Vecchio, F.J. (1990), “Reinforced concrete membrane element formulation”, *J. Struct. Eng., ASCE*, **116**(3), 730-750.
- Wang, J. (2006), “Constitutive relationships of prestressed concrete membrane elements”, Ph.D. Dissertation, Department of Civil and Environmental Engineering, University of Houston, Houston, TX.
- Zhong, J. (2005), “Model based simulation of reinforced concrete plane stress structures”, Ph. D. Dissertation, Department of Civil and Environmental Engineering, University of Houston, Houston, TX.
- Zhu, R.H. (2000), “Softened membrane model for reinforced concrete elements considering poisson effect”, Ph. D. Dissertation, Dept. of Civil and Environmental Engineering, University of Houston, Houston, TX.
- Zhu, R.H., Hsu, T.T.C. and Lee, J.Y. (2001), “Rational shear modulus for smeared crack analysis of reinforced concrete”, *Struct. J. American Concrete Institute*, **98**(4), 443-450.
- Zhu, R.R.H. and Hsu, T.T.C. (2002), “Poisson effect of reinforced concrete membrane elements”, *Struct. J. American Concrete Institute*, **99**(5), 631-640.